Computers in Biology and Medicine 39 (2009) 545 – 553

Contents lists available at ScienceDirect

Computers in Biology and Medicine

journal homepage: www.elsevier.com/locate/cbm

2D image registration using focused mutual information for application in dentistry

W. Jacquet[a,*], E. Nyssen[c], P. Bottenberg[d], B. Truyen[c], P. de Groen[b]

[a]Vrije Universiteit Brussel, Department of Mathematics, Operational Research, Statistics, and Information Systems, MOSI, Pleinlaan 2, B-1050 Brussels, Belgium
[b]Vrije Universiteit Brussel, Department of Mathematics, DWIS, Pleinlaan 2, B-1050 Brussels, Belgium
[c]Vrije Universiteit Brussel, Department of Electronics and Informatics, ETRO, Pleinlaan 2, B-1050 Brussels, Belgium
[d]Vrije Universiteit Brussel, Dental School, COPR, Laarbeeklaan 101, 1090 Brussels, Belgium

ARTICLE INFO

Article history:
Received 14 July 2008
Accepted 25 March 2009

PACS:
07.05.Pj
07.05.Rm
87.57.−s
87.57.Gg

Keywords:
Image registration
Registration criteria
Information theory
Entropy
Mutual information
Digital subtraction radiography
Piecewise rigid
Dentistry

ABSTRACT

Spatial alignment of image data is a common task in computer vision and medical imaging. This should preferentially be done with minimal intervention of an operator. Similarity measures with origin in the information theory such as mutual information (MI) have proven to be robust registration criteria for this purpose. Intra-oral radiographs can be considered images of piecewise rigid objects. Teeth and jaws are rigid but can be displaced with respect to each other. Therefore MI criteria combined with affine deformations tend to fail, when teeth and jaws move with respect to each other between image acquisitions. In this paper, we consider a focused weighing of pixels in the reference image. The resulting criterion, focused mutual information (FMI) is an adequate tool for the registration of rigid parts of a scene. We also show that the use of FMI is more robust for the subtraction of lateral radiographs of teeth, than MI confined to a region of interest. Furthermore, the criterion allows the follow-up of small carious lesions when upper and lower jaw moved between the acquisition of test and reference image.

1. Introduction

Pixel/voxel based similarity measures such as mutual information (MI) [1] are frequently used criteria for the registration of images in a wide variety of clinical applications [2]. They allow for fully automated alignment. Segmentation, feature extraction, or other types of preprocessing are not required for the calculation of MI similarity measures.

In this paper we study registration of images of a scene consisting of a number of rigid parts (objects) that may be more or less mobile relative to each other. When the variation in the geometry between successive image acquisitions is small enough, an affine transformation, aligning the images, can be found. If the relative position of these rigid parts changes between image acquisitions, it may become impossible to find one single affine transformation, aligning the image correctly for all parts at once. An MI based similarity measure will tend to propose an affine transformation, searching an optimal trade-off between the registration of the different parts. Traditional MI weighs the gray value combinations of the pixels equally. We propose a focused mutual information (FMI): a non-uniformly weighted MI that emphasises the contribution in the neighbourhood of the focus, and reduces that of regions possibly hampering the alignment.

One area of application is intra-oral radiography. Intra-oral radiography in combination with digital subtraction radiography (DSR) facilitates the detection and evolution of periodontal diseases and alveolar bone changes [3]. In cariology, DSR is a potentially interesting technique for the follow-up of small lesions [4] in order to decide between further observation in combination with adequate preventive measures (non-intervention) therapy [5] or a restorative treatment (intervention). Lehmann et al. [6] used dental radiographs of a dry mandibula under controlled geometrical circumstances to compare eight similarity measures for DSR. Although MI was not yet included in this study, it was already an entropy based measure that outperformed the other similarity measures. The application of DSR to the follow-up of carious lesions is presently explored to a lesser extent because of the small size of the lesions and the resulting very subtle changes in gray level. However, it would put the clinician's decision on a much sounder basis than the purely visual comparison of two consecutive X-ray images. The variation in geometry of the X-ray source, the patient, and the intra-oral sensor most often results

* Corresponding author. Tel.: +32 2 629 19 65.
E-mail address: wjacquet@vub.ac.be (W. Jacquet).

0010-4825/$ - see front matter © 2009 Elsevier Ltd. All rights reserved.
doi:10.1016/j.compbiomed.2009.03.011

in irreversible distortions from one image to the other [7]. If the variation in geometry is sufficiently small, a satisfactory alignment can be obtained using an affine transformation. The variation can only be small enough if the X-rayed scene can be considered rigid. This is not always the case in dental applications because of natural tooth mobility, orthodontic treatment or movement of the lower jaw with respect to the upper jaw. A natural reflex is to reduce the test image to a region of interest (ROI) that includes "only" the object to be aligned [8]. Most often, a rectangular ROI is used for simplicity. ROIs only encompassing the object of interest require more interaction or extensive calculation. In other cases, the object of interest cannot be clearly defined or delimited. ROI alignment in combination with an MI criterion is a special case of FMI registration, in which only weights zero and one are allowed. The focus region in FMI may be considered as a kind of soft "region of interest", where the comparison functional itself is adapted to the area of study and down-weighted smoothly outside this domain. It differs from conventional ("hard") ROI methods, in that it does not cut parts from images for registration, e.g. as in [9], where the size of the cut and the (artificial) discontinuity caused by it, strongly influences the quality of the registration. The FMI alignment is much less computationally intensive than the free boundary approach of [10], where the location of the boundary itself is part of the optimization. Moreover, the quest of conventional ROI-registration in general is to detect an object in otherwise unrelated backgrounds, whereas the background in our problem is significant, but may be distorted at somewhat larger distances. After the introduction of FMI, the technique is demonstrated using examples from dental research and clinical practice. Then we will illustrate that FMI is more robust than ROI, and that the result of FMI registration is not critically dependent on the choice of parameters. To conclude, an application in dentistry will demonstrate the practical applicability of FMI.

2. Information measures

In what follows, we will consider 2D gray scale images as arrays of pixels. A function, assigns one of K gray value bins $\{1,\dots,K\}$ to each array element. Let u and v be two images. We will refer to u as the reference image and v as the test image. Let $\mathscr{A}$ be a class of smooth bijective mappings from $\mathbb{R}^2$ to $\mathbb{R}^2$. The idea of image registration is to find a spatial transformation $T \in \mathscr{A}$ such that image u and the transformed image, $v_T = v \circ T^{-1}$, are as similar as possible. Given a measure I of similarity between images, optimal registration can be defined as the problem to find the transformation T that maximises this measure, i.e.

$$\arg\max_{T\in\mathscr{A}} I(u, v_T).$$

In our experiments we will restrict ourselves to affine transformations. The quality measure I of a transformation T is directly based on the combined 2D gray map g_T,

$$g_T(m,n) := (\widehat{u}(T(m,n)), v(m,n)), \tag{1}$$

defined for all nodes (m,n) of the test image satisfying $T(m,n) \in A$ (the support of the reference image)—see Fig. 1, and where $\widehat{u}(T(m,n))$ is a gray value obtained through interpolation from known values of u at nodes of u neighbouring $T(m,n)$.

Several interpolating techniques can be applied. We will adopt bilinear interpolation—see the following equation:

$$\widehat{u}(T(m,n)) = \sum_{i=1}^{4} u(n_i) w_i, \tag{2}$$

(illustrated by Fig. 1) where n_1, n_2, n_3 and n_4 are the nodes of u surrounding $T(m,n)$ and w_i is the area of the rectangle opposite to n_i for $i = 1,\dots,4$—see Fig. 2.

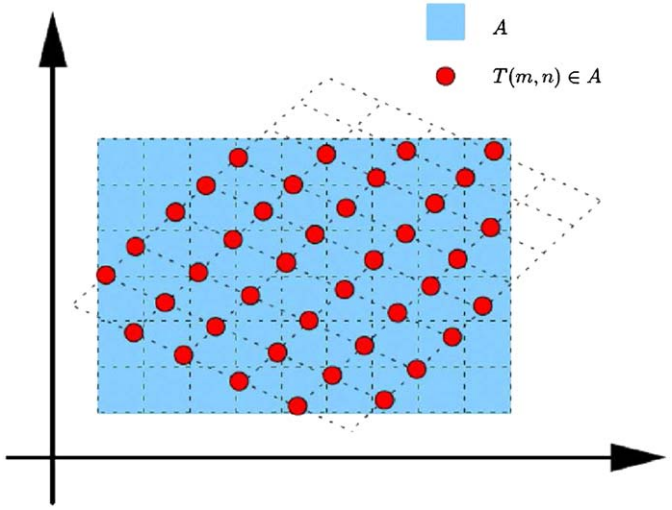

Fig. 1. Mapping of the test image pixels on the reference image through transform T.

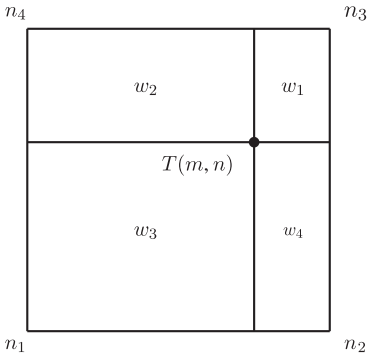

Fig. 2. Bilinear interpolation.

2.1. Entropy of images

The Shannon entropy measures uncertainty about a precise outcome of an experiment, linked to a probability distribution. Given a discrete probability model with probabilities $p_1, p_2, \dots, p_n$, the Shannon entropy H [11] is defined as

$$H(p_1, p_2, \dots, p_n) := -\sum_{i=1}^{n} p_i \ln p_i. \tag{3}$$

In order to define the joint entropy of two images, we consider the function counting the number of occurrences of a gray value combination in the intersection of the reference image with the transformed test image:

$$\begin{aligned} C_T(k,l) &:=]\{(m,n) | T(m,n) \in A \wedge (k,l) \\ &= (\widehat{u}(T(m,n)), v(m,n))\}. \end{aligned} \tag{4}$$

In the 2D gray value map of two perfectly aligned copies of the same picture, both components of the gray value map are always equal, and hence the frequency of occurrence of unequal components is zero. Optimal registration of two images of the same scene taken in an almost identical measurement setup would lead to all "off diagonal" elements being "small" and at least one of the "diagonal elements" being "large". "Small" and "large" are to be related to the number of pixels in the overlap. Therefore we divide C_T by the number of pixels in the intersection of reference image and transformed test image to eliminate the dependency on the image size.

The result is a 2D probability distribution, called the joint probability of the images:

$$p_{kl} := \frac{C_T(k,l)}{\sum_{ij} C_T(i,j)} \quad \text{joint probability,}$$
$$p_{k\bullet} := \sum_l p_{kl} \quad \text{marginal distribution linked to the reference image,}$$
$$p_{\bullet l} := \sum_k p_{kl} \quad \text{marginal distribution linked to the test image.} \tag{5}$$

The joint entropy $H(u, v_T)$ of two images u and v_T is the Shannon entropy of the joint probability of the images. The entropy $H(u)$ of the reference image is the Shannon entropy of $p_{k\bullet}$, the entropy $H(v_T)$ is the Shannon entropy of $p_{\bullet l}$. Although there might be a confusion between the notation for the entropy $H(p_1, p_2, \ldots, p_n)$ used by Shannon and the notation for the joint entropy $H(u, v_T)$ used in the imaging community we will keep both, the interpretation being obvious from the context. When two images are well aligned, but intensities of the same structure differ, the set of probabilities will not change, but those probabilities may be assigned to shifted gray value combinations. Hence, the Shannon entropy will not be affected since it is invariant under permutation of elements—see Eq. (3). Therefore the use of a similarity measure based on the entropy is a sensible option when the image acquisition modalities of the two images differ. In addition to the absence of preprocessing, this is a reason why entropy based similarity measures are popular in multi-modal registration applications at present.

2.2. Focused mutual information

The mutual information I of the reference image u and the transformed image v_T is defined as [12,13]

$$MI(u, v_T) := H(u) + H(v_T) - H(u, v_T), \tag{6}$$

where the entropies are calculated over the region of overlap.

The normalised mutual information Y introduced in [14] balances the sum of marginal entropies and the joint entropy to become a criterion more robust to changes in overlap than MI,

$$Y(u, v_T) := \frac{H(u) + H(v_T)}{H(u, v_T)}, \tag{7}$$

where the entropies are calculated over the region of overlap.

Let (k,l) be a gray value combination and let $D(k,l)$ denote the set of points (m,n) in the test having value k as interpolated gray value of the reference image at $T(m,n)$ and value l as gray value of the test image at (m,n),

$$D(k,l) := \{(m,n) | T(m,n) \in A \wedge (k,l) = (\widehat{u}(T(m,n)), v(m,n))\}.$$

Let $f(i,j)$ be a set of weights normalised to a probability chosen such that the highest probabilities coincide with the regions of the reference image corresponding to the rigid part of the scene we want to register. We define:

$$C_T(k,l) := \sum_{(m,n)\in D(k,l)} 1 \tag{8}$$

counting the number of elements of each $D(k,l)$,

$$W_T(k,l) := \sum_{(m,n)\in D(k,l)} f(m,n) \tag{9}$$

counting the weights of all elements of each $D(k,l)$,

$$p_{kl} := \frac{C_T(k,l)}{\sum_{ij} C_T(i,j)} \tag{10}$$

(uniform) joint probability of the images,

$$\pi_{kl} := \frac{W_T(k,l)}{\sum_{ij} W_T(i,j)} \tag{11}$$

focused joint probability of the images.

The following *FMI* estimators will be used:

$$MI_f(v, v_T) = H_f(u) + H_f(v_T) - H_f(u, v_T),$$

respectively,

$$Y_f(v, v_T) = \frac{H_f(u) + H_f(v_T)}{H_f(u, v_T)}, \tag{12}$$

where

$$H_f(u, v_T) = -\sum_{kl} \pi_{kl} \log(\pi_{kl}),$$
$$H_f(u) = -\sum_{k} \pi_{k\bullet} \log(\pi_{k\bullet}),$$
$$H_f(v_T) = -\sum_{l} \pi_{\bullet l} \log(\pi_{\bullet l}).$$

This estimator is analogous to the conventional or uniform MI estimator, in which the uniform probabilities—see Eq. (10)—are replaced by the weighted ones—see Eq. (11).

In all experiments we will use a focus distribution as normalised convex combination $f = \sum a_i f_i$ of a finite number of Gaussian density functions f_i. Defining such a focus distribution consists of choosing the focus centres and the standard deviations when the Gauss distributions are chosen to be isotropic. The success of an FMI based alignment will depend on an appropriate choice of the set of weights. In all experiments "FMI" will refer to the model described here, in contrast to ROI. In the robustness experiments, normalised focused mutual information is used to reduce possible overlap effects. We will still refer to registration, based on normalised mutual information, as an "FMI" registration.

3. Experiments

3.1. Numerical experiments

As an illustration, we use two images with 128 gray values and 256×256 pixels of a cup that contains the head of a cat—see Fig. 3. In the test image the cat is moved relative to the cup. The optimization is performed using the DIRECT method implemented by Finkel [15]. When (standard) MI is used as registration criterion, the cat is placed over the cup and vice versa—see Fig. 4. When only the cat is focused, with focus parameters as in Table 1, the cat is nearly perfectly aligned; errors are in the order of magnitude

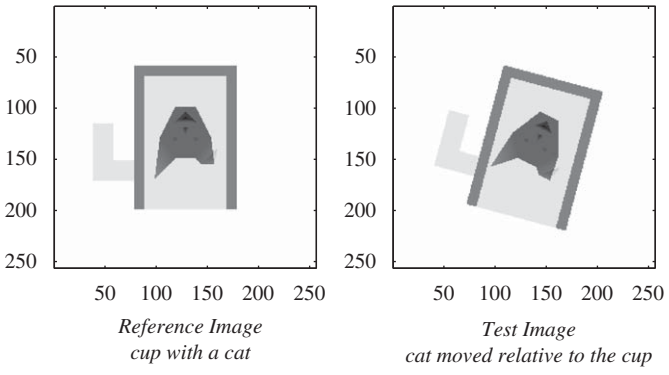

Fig. 3. Pictures with cup and cat.

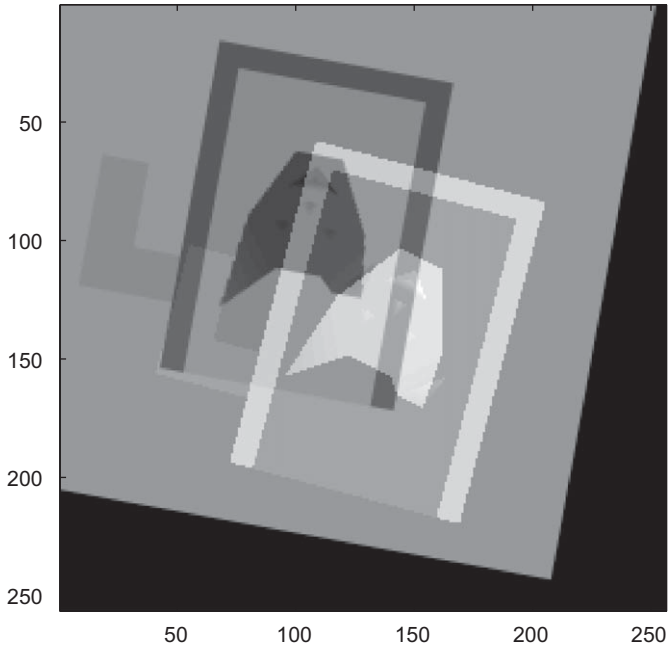

Fig. 4. Cup-cat subtraction image with (uniform) MI registration.

Table 1
Parameters of a single Gauss focus patch on the cat image (Fig. 5).

$Mean_x$	$Mean_y$	Var_x	Cov_{xy}	Var_y
128.5	128.5	20^2	0	20^2

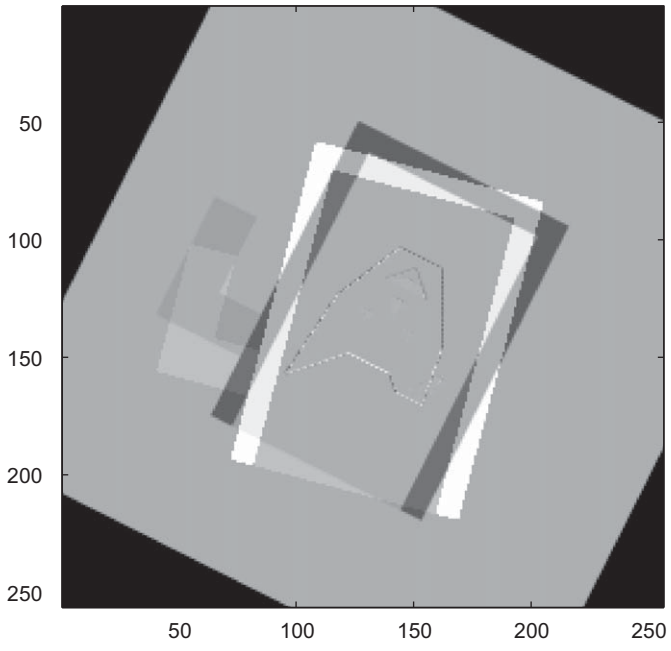

Fig. 5. FMI registration with focus on the cat.

of a pixel—see Fig. 5. When the corners of the cup image and the upper and lower part of the handle are focused, with focus parameters as in Table 2, the cup is aligned up to the order of one pixel—see Fig. 6.

Table 2
Parameters of the six Gauss focus patches on the peripheral elements of the cup image (Fig. 6).

$Mean_x$	$Mean_y$	Var_x	Cov_{xy}	Var_y
80	200	20^2	0	20^2
170	200	20^2	0	20^2
80	75	20^2	0	20^2
170	75	20^2	0	20^2
70	175	20^2	0	20^2
70	120	20^2	0	20^2

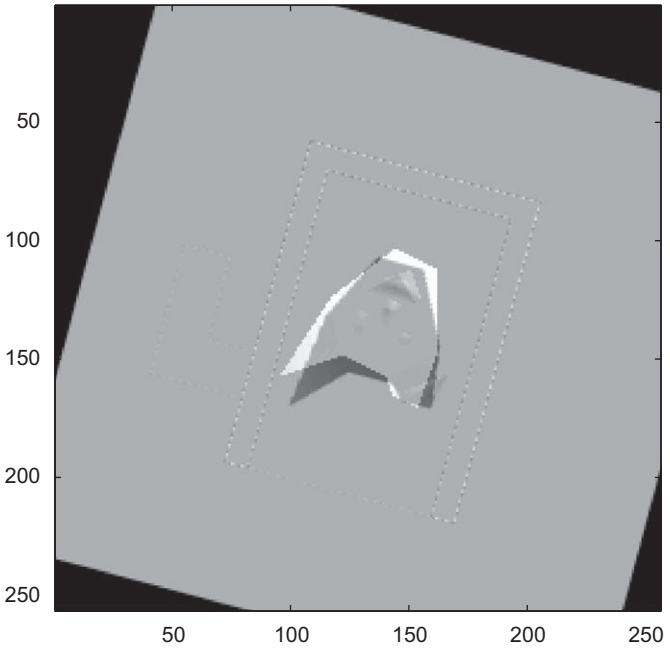

Fig. 6. FMI registration with focus on the cup.

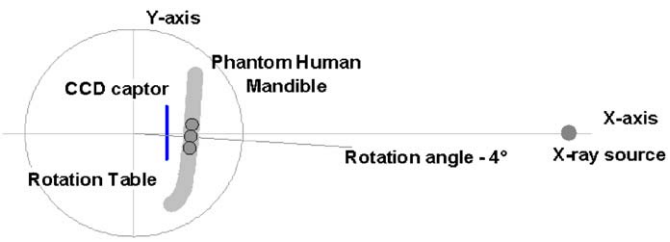

Fig. 7. Setup of the ROI—focus experiment.

3.2. Mandibular phantom experiments

A series of radiographs was made of a phantom set-up of a human mandible; contiguous (pre-)molars, centred around tooth 35 (second lower left premolar), were placed on a rotating stage between an X-ray source and a CCD captor—see Figs. 7 and 9. Images of the phantom were taken at angles ranging from -4° to 4° in steps of 0.5°, resulting in a set of 17 images. In a second series of 17 images, tooth 35 was displaced mesially with respect to the neighbouring teeth—see Fig. 10. Radiographs were recorded using a dental CCD captor (Gendex Visualix, and appropriate software VIXWIN 2000, Dentsply Italia s.r.l.). The images were stored as ⋆.tif files at a resolution of 640×488 pixels with 256 gray values. Registration was done with respect to tooth 35.

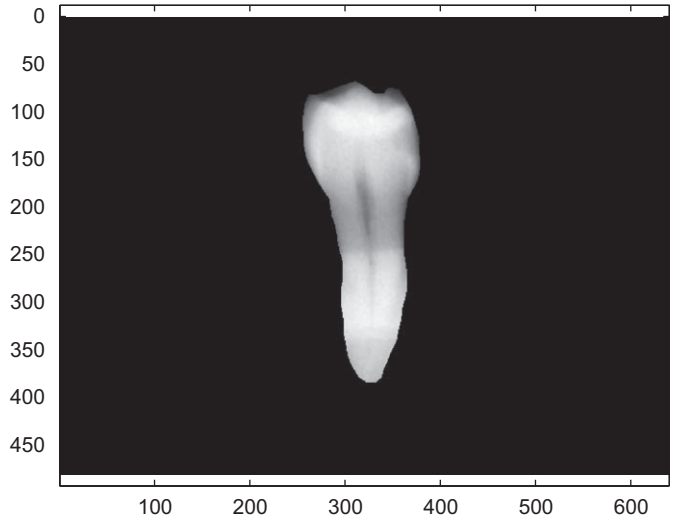

Fig. 8. Area delineating tooth 35.

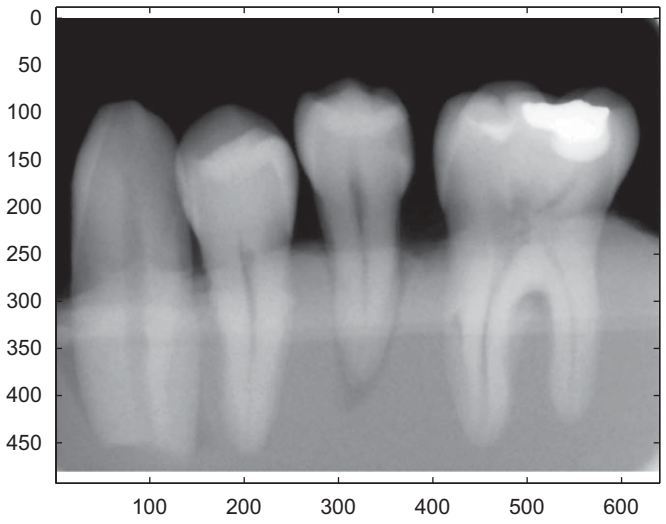

Fig. 10. Image of the phantom with tooth 35 displaced.

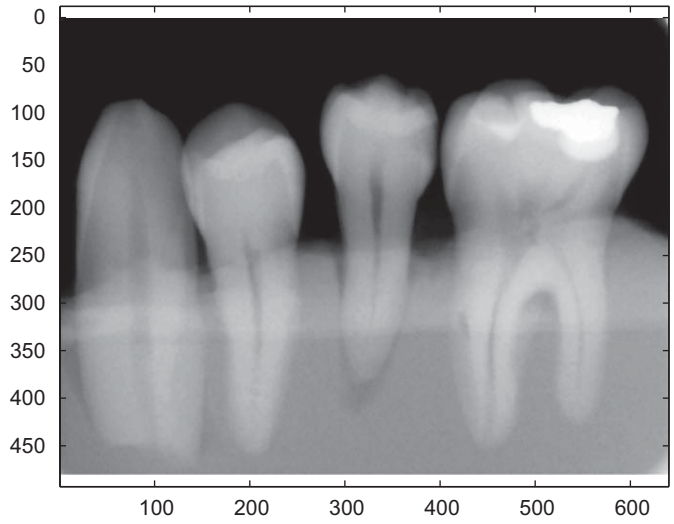

Fig. 9. Image of the phantom.

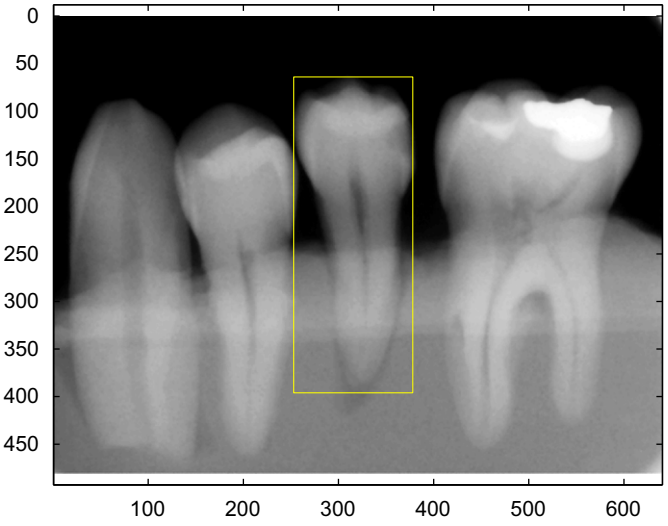

Fig. 11. Initial rectangular region containing tooth 35.

In such a standardised environment the quality of the alignment of tooth 35 can be assessed by the square root of the sum of squared differences (SDDI) between reference image and transformed test image. For all aligned pairs the SDDI is evaluated over the area of tooth 35, as delineated in Fig. 8.

In a first experiment (Section 3.2.1), we compare the robustness of both ROI and FMI registration with respect to a size-of-domain parameter. The image of the mandibular phantom in the initial position is used as reference image. In the test image tooth 35 is displaced mesially and the mandibular is rotated over 0.5°. The slight rotation simulates a small misalignment error in the background teeth surrounding tooth 35.

In a second experiment (Section 3.2.2), we compare the alignment of all image pairs with corresponding rotation angles using both FMI and ROI with optimal size-of-domain parameters.

In a third experiment (Section 3.2.3), we test the robustness of FMI alignment with respect to deviations in focus centres. We use the same reference and test images as in the first experiment (Section 3.2.1).

3.2.1. Robustness of FMI versus ROI

ROI registration: The smallest rectangle around tooth 35 consisting of 125×332 pixels was taken as the reference ROI—see Fig. 11. Its width was shrunk and extended with respect to the centre in constant steps of two pixels, and its height was adapted proportionally. This resulted in a set of nested windows of increasing size with a width ranging from 3 to 201 pixels. For each of these cropping windows, the optimal alignment using Studholme Y—see Eq. (7)—as criterion was computed. In Fig. 12 the dotted line shows the SDDI of the resulting alignments as a function of the width of the ROI. To speed up searching each alignment, a least squares initial guess was calculated from four reference points on tooth 35 in test and reference image.

FMI registration: On the central (vertical) axis of tooth 35 in the reference image Fig. 13, eight (more or less) equidistant foci are chosen and FMI registrations are calculated with standard deviations ranging from 1 to 101 pixels in steps of 2. In Fig. 12 the solid line shows the SDDI of the resulting alignments as a function of the standard deviation.

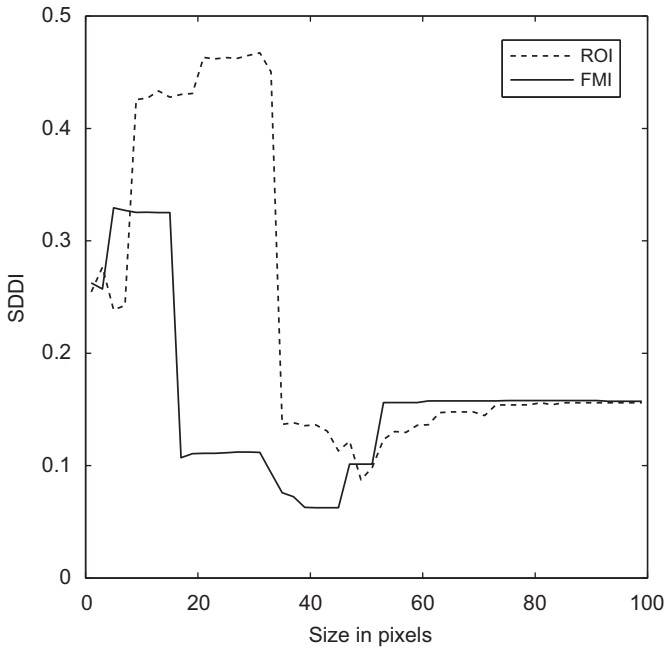

Fig. 12. SDDI as function of ROI size (dashed) and focus standard deviation (solid).

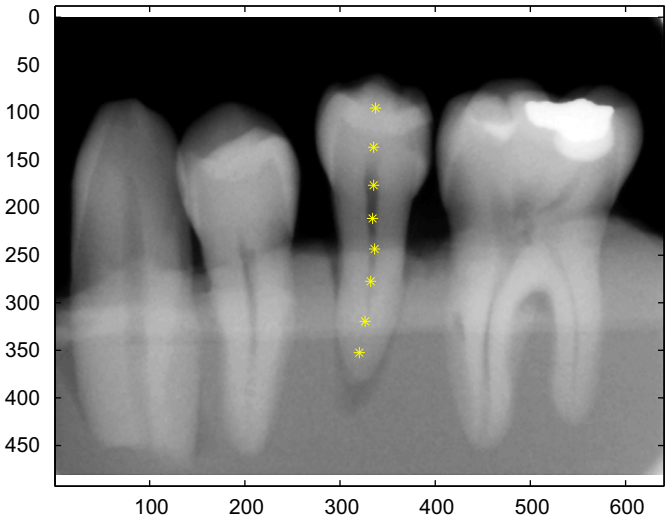

Fig. 13. Focus centres reference image.

Comparison: The best FMI focus standard deviation is 43 pixels and the corresponding SDDI is 30% smaller than the SDDI of the registration at the best ROI size.

3.2.2. Overall performance FMI versus ROI

For each of the 17 image pairs with corresponding rotation angles the procedure of the first experiment (Section 3.2.1) was repeated to obtain ROI and FMI alignment both with optimal size-of-domain parameters.

Comparison: In 15 out of the 17 image pairs the minimum SDDI in FMI registration was smaller than the minimum for ROI-registration. This result is statistically significant (Wilcoxon $N = 17$, $Z = -3.290$ and $p = 0.001$).

3.2.3. Robustness to deviation in focus point indication

FMI registration: The FMI registration of the first experiment with a focus standard deviation of 43 pixels (Section 3.2.1) was repeated $N = 50$ times. At each repetition the focus centres were perturbed according to a normal distribution with variance covariance matrix $\Sigma = 10^2 I$.

Comparison: The minimal SDDI was 0.0626, the mean 0.068 and the standard deviation 0.011. In 90% of the cases the SDDI alignment based on the perturbed focal centres was better than the minimal SDDI found for ROI alignment in the first experiment (SDDI=0.0874). In 10% of the cases the alignment based on the perturbed focal centres was superior to the unperturbed case.

3.2.4. Conclusions

The FMI registration shows to be more robust to changes in focus standard deviation than the ROI with respect to changes in ROI size. In the second experiment, FMI alignment shows a better overall performance than ROI alignment. The last experiment demonstrates the robustness of FMI with respect to deviations in focal centres.

4. Application in dentistry

As a practical illustration we use in vivo bitewing radiographs, acquired at two years interval. The images are taken using a Philips (now Gendex) X-ray generator operating at 65 kVp and 20 mA, with an exposure time of 0.32 s on an AGFA Dentus E-type radiographic film. After development (Dürr Periomat, Dürr, Bietigheim-Bissingen, Germany), images are scanned at a resolution of 520×836 pixels with 192 gray values. Except for the use of conventional beam-aiming devices (Rinn XCP, Rinn, Elgin IL, USA), no custom-made bite-blocks [16] were used. In the clinical procedure, care was taken to obtain a matching exposure geometry. When comparing both X-ray images in Fig. 14, it can be noted that the patient has shifted her lower jaw forward while holding the bite-block. Furthermore, the bite-block and film were shifted backwards with regards to the reference image, resulting in a translation of the central beam distally by about 8 mm. The aim of the X-ray examination was to ascertain whether the carious lesions on the distal surface of the lower left first molar (36) and the mesial surface of the lower second molar (37) had increased in size. In this case, a restorative treatment should be indicated instead of non-intervention therapy. Simple observation of reference and test image learns that the latter is much darker than the former. The gray value histograms of the reference image and the test image are similar, yet shifted—see Fig. 15. Since MI and FMI both are insensitive to changes in intensity, the alignment is done without correction. The subtraction image and its interpretation will be influenced by an intensity change. Figs. 18 and 21 are subtraction images without transformation. To compensate for intensity differences between the images when subtracting, we applied a linear transformation to the test image equalising first and second order moments, resulting in the subtraction images shown in Figs. 19 and 22. The choice of the foci is done manually with a visual check by looking at the product of the reference image and the focus distribution—see Figs.17 and 20.

At first, we focus on tooth 36 with focus parameters as in Table 3. The teeth of the upper jaw are not aligned—see Fig. 18. A small change on the outer contour of the distal surface of tooth 36 can be seen. This is probably due to residual alignment errors. Neither on tooth 36 nor on tooth 37, noticeable differences in the carious lesions can be seen. It could be concluded that the lesions are stable and do not need immediate restorative treatment.

When focussing on the upper left first molar (26) with focus parameters as in Table 4, the upper jaw is well aligned—see Fig. 21. In the upper jaw, a perfect alignment can be seen on the distal aspect of tooth 26. At the mesial side of tooth 26, a contour is visible, due to residual misalignment. This is more pronounced for the pre-molars,

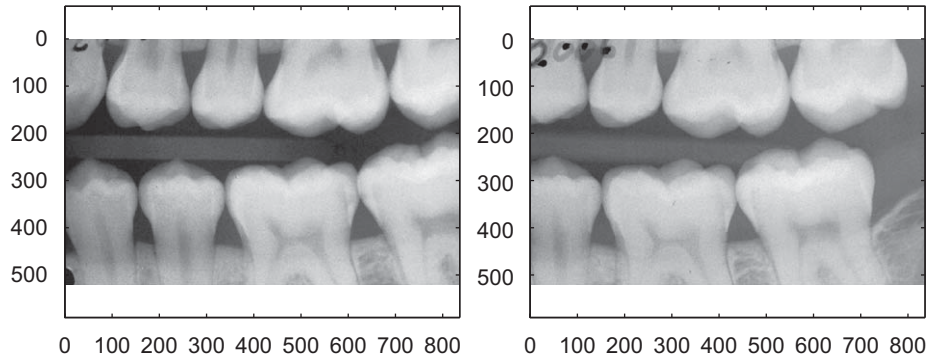

Fig. 14. Reference image (left) and test image (right).

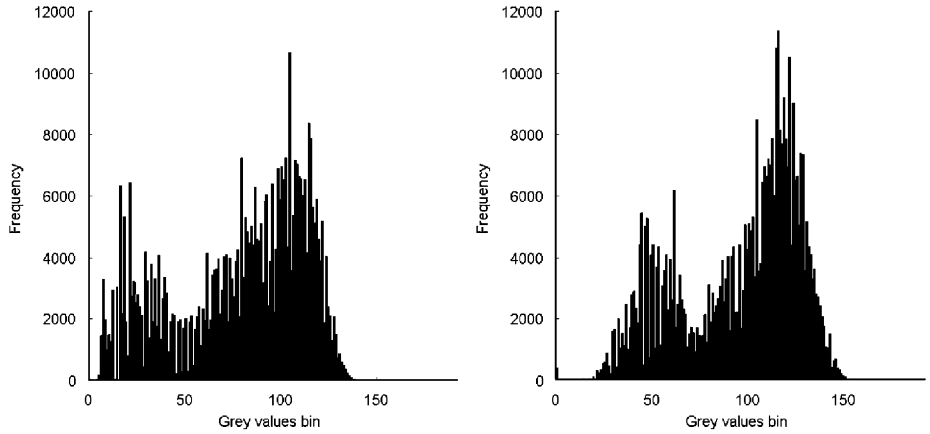

Fig. 15. Histograms of reference image (left) and test image (right), Fig. 14.

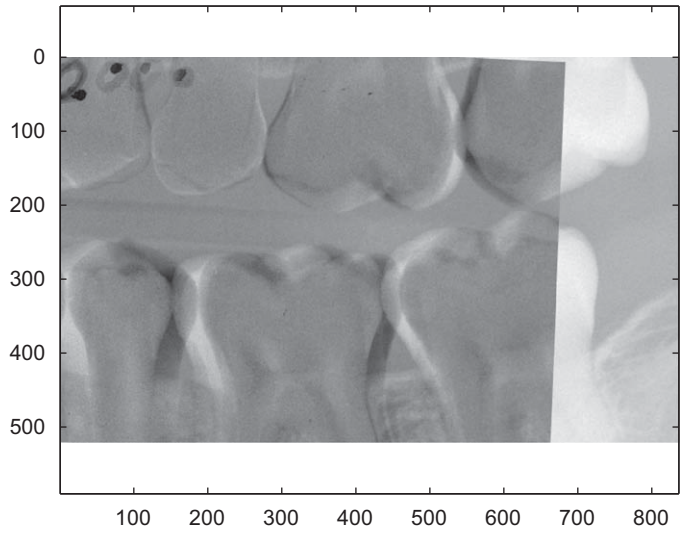

Fig. 16. Subtraction image using uniform MI.

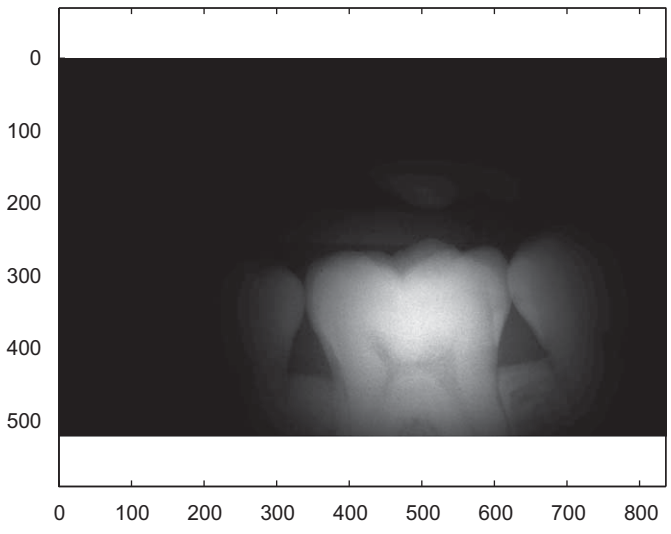

Fig. 17. Product of focus over the lower left first molar (36) and reference image gray values.

showing a white mesial contour and a black distal contour. This phenomenon was most probably due to the rotation of the jaw or the X-ray source with respect to the film between the acquisition of reference image and test image. No relevant changes in enamel or dentine of tooth 26 can be observed.

A fully automatic registration using (uniform) mutual information as criterion results in the alignment of the upper jaw—see the subtraction image Fig. 16. This alignment is not good enough to draw conclusions regarding the evolution of existing caries or the detection of new lesions.

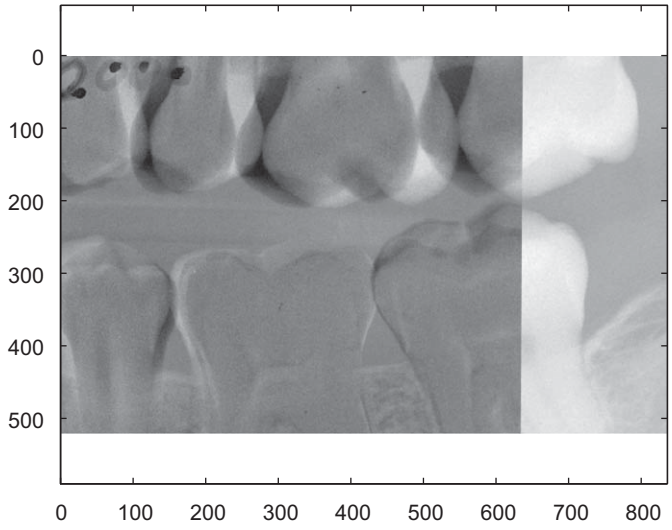

Fig. 18. Subtraction image using FMI with focus on lower left first molar (36).

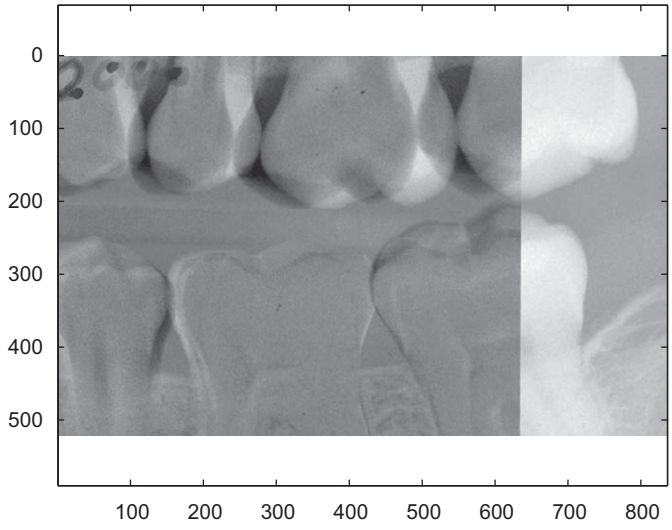

Fig. 19. Intensity corrected subtraction image using FMI with focus on the lower left first molar (36).

5. Discussion and conclusions

Registration algorithms using affine transformations and uniform information measures may often fail to align images of piecewise rigid objects, or may align only one part of the image, when the geometry of rigid parts changes between image acquisitions. Moreover, the registered region will not necessarily be the part we want to track. Even if the object of interest is aligned, the quality of the registration may be suboptimal, due to the attempt of the algorithm to align also the rest of the scene. When a focus is applied, we can direct the registration towards the region of interest. This enables shifting the focus from tooth to tooth, according to the diagnostic needs. The implication is that the procedure is semi-automatic at best. Without the practitioner, it is impossible to decide which part of the piecewise rigid object needs to be aligned. However, the procedure is not as elaborate and sensitive to small errors as the indication of reference points. The focus has to be determined for one image only, either in the reference image or in the test image. An alternative classical approach consists of reducing the test image to a region of interest containing "only" the object to be aligned. The experiments, conducted in this paper, indicate that the use of an ROI is less robust to changes in ROI size, than FMI is to changes in focus size. Moreover, the use of an ROI is less accurate than the application of FMI. Finally, the accuracy of the location of the foci is not critical to the quality of the registration. Therefore, this technique can be of interest for the subtraction of dental intraoral radiographs.

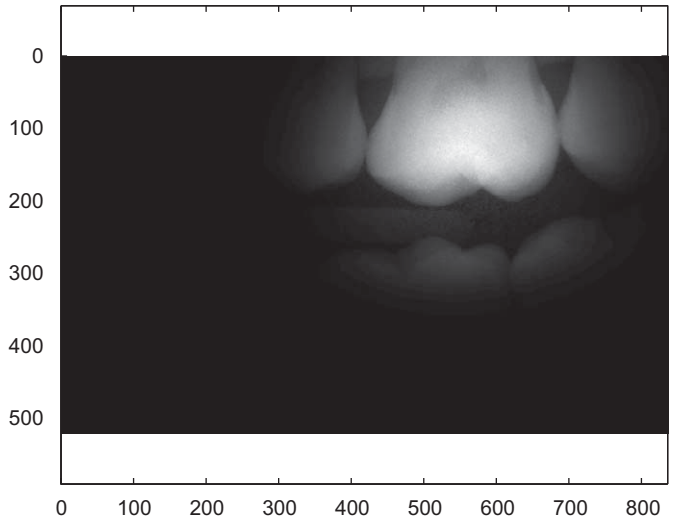

Fig. 20. Product of focus over the upper left first molar (26) and reference image.

Table 3
Parameters of the Gauss focus over the lower left first molar (36)—see Fig. 17.

$Mean_x$	$Mean_y$	Var_x	Cov_{xy}	Var_y
330	500	70^2	0	100^2
420	500	70^2	0	100^2

Table 4
Parameters of the Gauss focus over the upper left first molar (26)—see Fig. 20.

$Mean_x$	$Mean_y$	Var_x	Cov_{xy}	Var_y
70	570	70^2	0	100^2
170	550	70^2	0	100^2

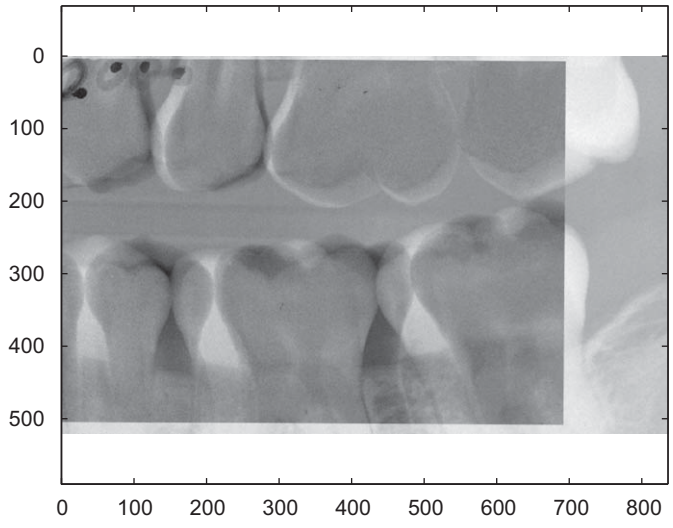

Fig. 21. Subtraction image using FMI with focus on the upper left first molar (26).

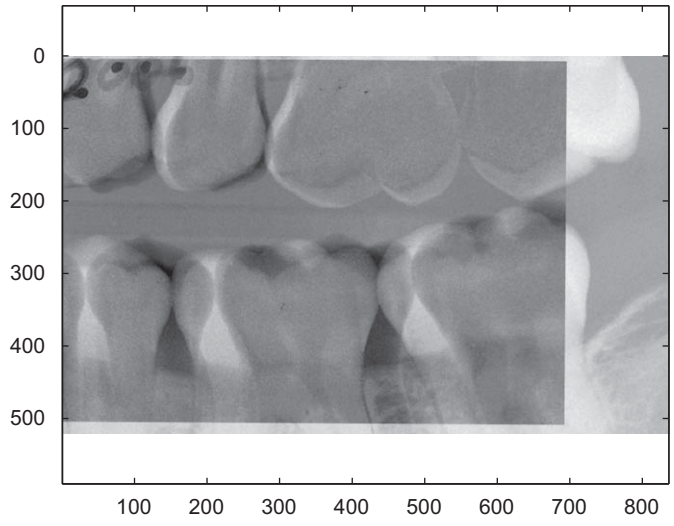

Fig. 22. Intensity corrected subtraction image using FMI with focus on upper left first molar (26).

Conflict of interest statement

None declared.

Acknowledgements

This research was partially funded by (1) FWO, Fund for Scientific Research—Flanders, Belgium (G.0304.04), (2) Ministry of the Flemish Community—Science, Innovation and Media Department Science and Innovation Administration, Belgium and Science Division, Science Division, State Committee for Scientific Research, Poland (BWS03/01, BWS04/11, BWS05/06) and (3) Research Council Vrije Universiteit Brussel—VUB, Brussels, Belgium (OZR742, OZR1109).

No funding organisation was involved in the study design, in the collection, analysis and interpretation of data, in the writing of the manuscript nor in the decision to submit the manuscript for publication.

References

[1] P. Viola, W.M. Wells, Alignment by maximization of mutual information, Med. Image Anal. 1 (1) (1995) 17–34.
[2] F. Maes, D. Vandermeulen, P. Seutens, Medical image registration using mutual information, Proc. IEEE 91 (10) (2003) 1699–1722.
[3] A. Mol, Imaging methods in periodontology, Periodontology 2000 34 (2004) 34–48.
[4] F. Haiter-Hero, R.I. Ferreira, C.P.M. Tabchoury, F.N. Boscolo, Linear and logarithmic subtraction for detecting enamel subsurface demineralization, Dentomaxillofac. Radiol. 34 (2005) 133–139.
[5] E.A.M. Kidd, J.P. Amerongen, The role of operative treatment, in: O. Fejerskov, E.A.M. Kidd (Eds.), Dental Caries, Blackwell Munksgaard, Oxford, UK, 2003.
[6] T. Lehmann, A. Sovakar, W. Schmitt, R. Repges, A comparison of similarity measures for digital subtraction radiography, Comput. Biol. Med. 27 (2) (1997) 151–168.
[7] R.L. Webber, U.E. Ruttimann, R.A. Groenhuis, Computer correction of projective distortions in dental radiographs, J. Dent. Res. 63 (8) (1984) 1032–1036.
[8] W.J. Yi, H.S. Heo, S.S. Lee, S.C. Choi, S.B. Lee, K.H. Huh, Automatic noise robust registration of radiographs for subtraction using strategic local correlation: an application to radiographs of dental implants, Comput. Biol. Med. 35 (3) (2005) 247–258.
[9] W.J. Yi, M.S. Heo, S.S. Lee, S.C. Choi, K.H. Huh, ROI-based image registration for digital subtraction radiography, Oral Surg. Oral Med. Oral Pathol. Oral Radiol. Endod. 101 (2006) 523–529.
[10] F. Richard, L. Cohen, A new image registration technique with free boundary constraints: application to mammography, Comput. Vision Image Underst. 89 (2003) 166–196.
[11] C.E. Shannon, A mathematical theory of communication, Bell Syst. Tech. J. 27 (1948) 379–423 623–656.
[12] A. Collignon, Multi-modality medical image registration by maximization of mutual information, Ph.D. Thesis, Catholic University of Leuven, Leuven, Belgium, 1998.
[13] F. Maes, A segmentation and registration of multimodal medical images: from theory, implementation and validation to a useful tool in clinical practice, Ph.D. Thesis, Catholic University of Leuven, Leuven, Belgium, 1998.
[14] C. Studholme, D.L.G. Hill, D.J. Hawkes, An overlap invariant entropy measure of 3D medical image alignment, Pattern Recognition 32 (1999) 71–86.
[15] D.E. Finkel, DIRECT optimization algorithm user guide, NC 27695-8205, Center for Research in Scientific Computation, North Carolina State University, Raleigh, NC, March 2003.
[16] K.H. Huh, S.S. Lee, I.S. Jeon, W.J. Yi, M.S. Heo, S.C. Choi, Quantitative analysis of errors in alveolar crest level caused by discrepant projection geometry in digital subtraction radiography: an in vivo study, Oral Surg. Oral Med. Oral Pathol. Oral Radiol. Endod. 100 (2005) 750–755.

Wolfgang Jacquet is assistant professor at the VUB—Department of Mathematics, Operational Research, Statistics, and Information Systems—MOSI.

Edgard Nyssen is professor at the VUB—Department of Electronics and Informatics—ETRO.

Peter Bottenberg is professor at the VUB—Dental School—COPR.

Bart Truyen is researcher at the VUB—Department of Electronics and Informatics—ETRO.

Peter de Groen is professor emeritus at the VUB—Department of Mathematics—DWIS.